J. Electrochem. Sci. Eng. **12(4)** (2022) 799-813; https://dx.doi.org/10.5599/jese.1411

Open Access : : ISSN 1847-9286
https://pub.iapchem.org/ojs/index.php/JESE

Original scientific paper

Chemical vapor deposited graphene-based quasi-solid-state ultrathin and flexible sodium-ion supercapacitor

Mohammed Saquib Khan[1†], Preeti Shakya[1†], Nikita Bhardwaj[2], Deependra Jhankal[2], Atul Kumar Sharma[1], Malay Kumar Banerjee[3] and Kanupriya Sachdev[1,2,✉]

[1]*Materials Research Centre, Malaviya National Institute of Technology Jaipur, JLN Marg, Jaipur 302017, India*

[2]*Department of Physics, Malaviya National Institute of Technology Jaipur, JLN Marg, Jaipur 30201, India*

[3]*Research Chair, SGVU, Jaipur,302017, India*

Corresponding author: ✉*ksachdev.phy@mnit.ac.in; Tel.: 0141-2713382*

Received: June 17, 2022; Accepted: August 23, 2022; Published: September 9, 2022

Abstract

Flexible electronic devices find wide application in wearable electronics and foldable gadgets. This article reports chemical vapor deposited (CVD) few-layers graphene for a solid-state flexible supercapacitor device. Raman spectroscopy analysis reveals up to five layers in the graphene samples. Polyvinyl alcohol-Na_2SO_4 hydrogel membrane is used as a gel polymer electrolyte (GPE). 50 nm thick silver (Ag) deposited on polyethylene terephthalate (PET) through E-beam deposition served as the flexible current collector for the device. Galvanostatic charge-discharge (GCD) executed on the fabricated device to analyze its electrochemical performance yielded a specific areal capacitance of 15.3 mF cm^{-2} at 0.05 mA cm^{-2} current density. The obtained power density of the fabricated device is 0.53 µWh cm^{-2} at a power density of 25 µW cm^{-2}.

Keywords

Gel polymer electrolyte; E-beam deposition; flexible electronics; lightweight supercapacitor; chemical vapor deposition; few-layer graphene

Introduction

The technological advancement in wearable and bendable electronics has created the need for thin, lightweight, and flexible solid-state energy devices [1]. These electronic devices require energy storage, fast charging and discharging, and high energy density. Among several energy storage devices, supercapacitors are the potential candidate owing to their advantages such as long cycle life, fast charge-discharge rates, high power performance and low maintenance cost [2-12]. Carbon-

[†]Mohammed Saquib Khan and Preeti contributed equally to this work.

based materials (graphene, carbon nanotube, activated carbon, carbon fibres, 3D carbon aerogel, *etc.*) play a crucial role in electrochemical energy storage credited to their exceptional properties such as a large specific surface area for electrochemical double layer capacitance, optimisable structures, adjustable compositions/components and tunable physiochemical properties [13]. Graphene is a two-dimensional monolayer of graphite with sp^2 hybridized carbon atoms arranged in a unique honeycomb structure, exhibiting high conductivity, excellent thermal stability, and excellent mechanical strength and showing the possibilities in multiple electronic applications [14,15]. It has been widely utilized in electrodes because it consists large theoretical surface area of 2630 $m^2 g^{-1}$, good chemical stability, excellent thermal stability, and its capability to facilitate the acquisition of electrons or the transfer of holes on its two-dimensional surface [16]. Several synthesis methods are used for single-layer and multilayer graphene. Compared to others, chemical vapor deposition (CVD) has been considered the most favourable method to fabricate graphene layers [17-19] because it yields superior electrical conductivity in comparison to chemically produced graphene [20,21]. The quality of synthesized graphene through CVD is adequate for sensitive electronic applications, making it ideal for electrochemical applications due to its large single crystal, easy synthesis of single/few-layer graphene, and transfer to another substrate [22,23]. On the other hand, graphene sheets are tremendously susceptible to restacking of multiple 2D layers, which adversely affects the mobility of ions and reduces electrochemically active sites [25,25]. Holey graphene, which is graphene with a large number of holes, is an excellent solution to the restacking problem [26].

Sodium sulphate has been widely used as a neutral electrolyte in Na-ion energy storage devices owing to its eminent ionic conductivity (125 mS cm^{-1} in water) and environmental safety [27,28]. Due to the scarcity of lithium resources worldwide, sodium-ion-based supercapacitors gained a lot of research attention for developing a less expensive and superior performing alternative compared to lithium-ion supercapacitors [29]. Liquid electrolytes have been used in electrochemical energy storage due to their benefits, including high ionic conductivities and ability to make good contact with electrodes, but they have disadvantages, *viz*. corrosive, toxicity, leakage, combustion of organic electrolytes and demand for a huge packaging cost for flexible capacitors [30]. Compared to them, gel polymer electrolytes (GPE) provide the advantage of flexibility, easy fabrication, broad potential window, stretchability, better adhesiveness, and high ionic conductivity [31]. Polyvinyl alcohol (PVA) is an excellent choice owing to its nontoxicity, biodegradability, cost-effectiveness, compatibility, fast film-forming property, high dielectric constant, and excellent chemical stability [32].

Different flexible and non-flexible conducting substrate materials, like Ti foil, Ni foam, aluminium foil, carbon cloth, fabric coated with graphene, stainless steel foil, graphite foil, or carbon fibres, are used as current collector plates in supercapacitor applications [33]. Metallic current collectors normally used in energy storage devices are not useful in lightweight and flexible devices because of their limitations of high resistance, low flexibility, and massive weight [34]. To address this, silver-coated polyethylene terephthalate (PET) substrate through electron beam deposition has been demonstrated as a prominent choice for the fabrication of ultrathin, lightweight, and flexible super-capacitor devices, which provides a wide range of temperature stability (≈ up to 250 °C) [35-36]. However, due to its insulating nature, it requires to be metalized for its utilization as a current collector. Metallization on a flexible substrate shows excellent potential, allowing flexibility and high electrical conductivity. The choice of coating material includes metals such as Ag, Au, Cu, and Ni or carbon-based materials including graphene and carbon nanotubes (CNT). Silver is a transition metal that offers several advantages over other metallic current collectors, including higher conductivity,

environment friendliness, and good electrochemical stability for supercapacitor application [37,38]. In comparison to the conventional metallic current collectors, silver-coated PET reduces the series resistance, overall weight, and manufacturing cost of the device and provides enhanced flexibility and better electrochemical performance [37].

In this communication, we report an ultrathin, flexible and eco-friendly silver deposited PET substrate-based supercapacitor device with CVD-grown few-layer holey graphene electrodes. PVA – Na_2SO_4 quasi solid state hydrogel membrane was used as the separator-less electrolyte. Parallel plate supercapacitor devices were fabricated by sandwiching Na_2SO_4 – PVA hydrogel membranes as the quasi solid-state and flexible electrolyte. Herein, we synthesized the holey few-layer graphene using the chemical vapour deposition method as resolution of the restacking problem in few-layer graphene, which facilitates the ionic movement of the electrolyte in the supercapacitor electrode that leads to the reduction of charge transfer resistance of the supercapacitor device. In addition, holes in the graphene layer give access to the inner layers for electrochemical energy storage, improving the supercapacitor's specific capacitance. Nevertheless, it is believed that there are no reports till now on the investigations of an ultrathin and flexible supercapacitor device using CVD-based few-layer holey graphene on silver deposited PET (current collector) as the flexible electrodes in combination with Na_2SO_4 – PVA hydrogel membranes as the quasi-solid-state electrolyte.

Experimental

Chemicals and materials

Copper foil (99.7 %) thickness ≈ 0.1 mm was procured from Loba Chemie Pvt. Ltd., Mumbai, India. Argon gas (99.999%), methane gas (99.999 %) and hydrogen gas (99.999 %) were purchased from Ankur Speciality Gases & Technologies, Jaipur, India. Ferric chloride ($FeCl_3$ 99.99 %), Iso-Propanol Alcohol (IPA 99.9 %), hydrochloric acid (HCl 35 %), acetone (99.9 %) and anisole (99.7 %) were purchased from Merck Life Science Private Limited, Darmstadt, Germany. Silver powder (8-10 µm) (99.9 %) was purchased from Sigma Aldrich, Missouri, USA. Polyethylene terephthalate (PET, thickness ≈0.1mm) was purchased from Savita Scientific and Plastic Products Private Limited, Jaipur, India. Poly-methyl methacrylate granules (PMMA 98 %) molecular weight ≈15,000 were procured from HiMedia Laboratories, Thane, India.

CVD growth of few-layer graphene

The low-pressure chemical vapor deposition (LPCVD) technique was used to grow few-layer graphene (FLG). After the cloth polishing and HCl treatment, the copper foil was annealed at 800 °C in argon and hydrogen gas at the rate of 100 and 50 standard cubic centimetres per minute (SCCM), respectively, for 180 minutes. Methane gas is used as the carbon source, and the hydrogen and methane gas flow rates were 25 and 50 SCCM, respectively, during the growth phase. The pressure of the chamber was maintained at 20 kPa, and the growth time of graphene was 35 min at 950 °C (Figure 1). After the growth phase, the furnace was cooled down to room temperature.

E-beam deposition of silver on PET substrate

E-beam evaporation technique was used to deposit silver (99.99 %) of 50 nm thickness on PET (polyethylene terephthalate, 0.1 mm) substrates. The substrate temperature was maintained at 90 °C, controlled with a precision ± 0.5 °C, and the pressure inside the chamber was 10^{-4} Pa with a deposition rate of 0.5-1 nm s^{-1}. The quartz balance technique was used to monitor film thickness

during deposition. After thin film deposition, Ag-PET substrates were thermally annealed at 120 °C for 60 min in an argon atmosphere.

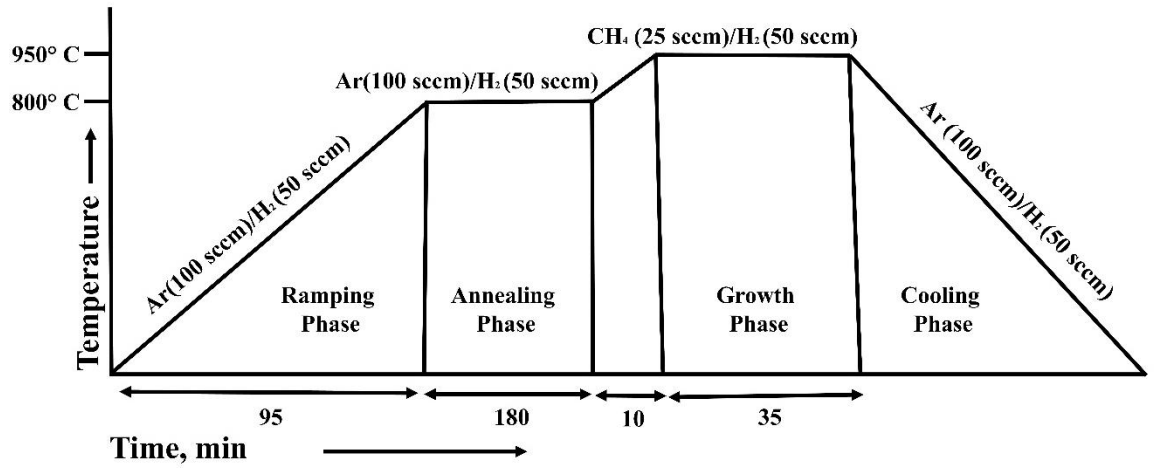

Figure 1. *Process parameters for few-layer graphene growth through CVD technique (rate of increase in temperature was 10 °C per minute and chamber pressure was ~20 kPa)*

Transfer process of few-layer graphene on the desired substrate

The CVD-grown graphene was transferred on the flexible silver/PET substrate through the copper etching technique, as reported in previous literature [39-42].

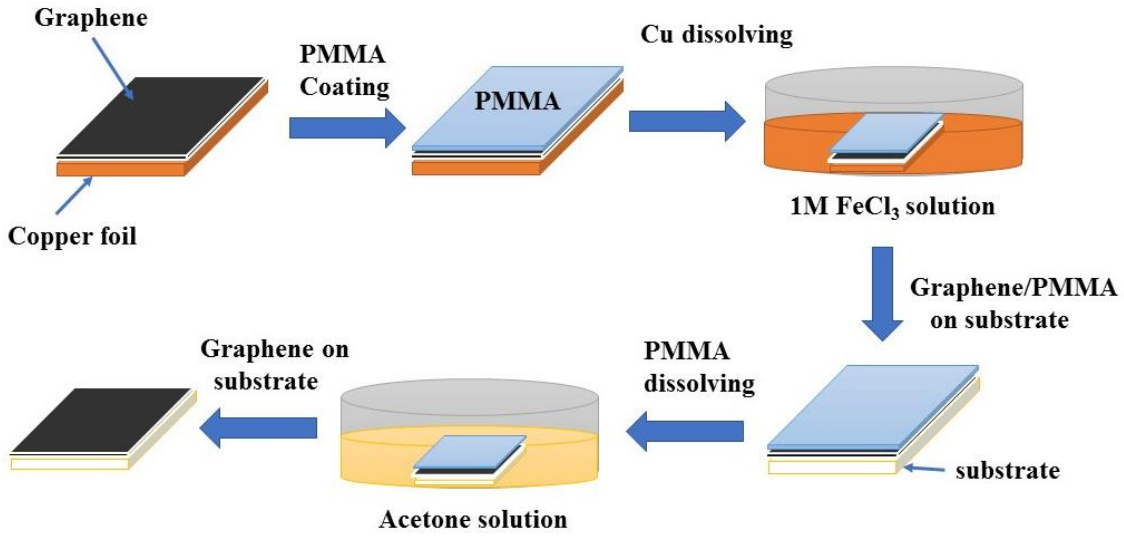

Figure 2. *Schematic of FLG transfer on the desired substrate*

The process begins with the spin coating of 10 % solution of PMMA in anisole on the samples. Ferric chloride solution (1 M) was used as a wet etchant to dissolve copper foil (thickness = 0.12 mm) and it takes approximately 15 – 20 minutes to completely dissolved (Figure 2), giving the floating PMMA-coated graphene sheets that are washed with DI water. These graphene sheets were placed on the silver-coated PET substrate and heated at 110 °C for 5 minutes. At last, acetone is used to remove PMMA coating, yielding only FLG on the substrate. The transferred FLG makes good adhesion with silver-coated PET substrate with appropriate uniformity.

Results and discussion

Raman spectroscopy analysis

In the Raman spectroscopy of graphene (Figure 3), the D band appearing at ≈1350 cm^{-1} arises due to out-of-plane vibrations attributed to the presence of structural defects [43]. The defects in few-layer graphene were quantified using the intensity ratio of the D-band to the G-band (graphitic band appearing at ≈1580 cm^{-1}) in the Raman spectrum (I_D/I_G) [44]. The I_D/I_G ratio of ≈0.25 indicates the presence of significant defect density in the synthesized samples [45].

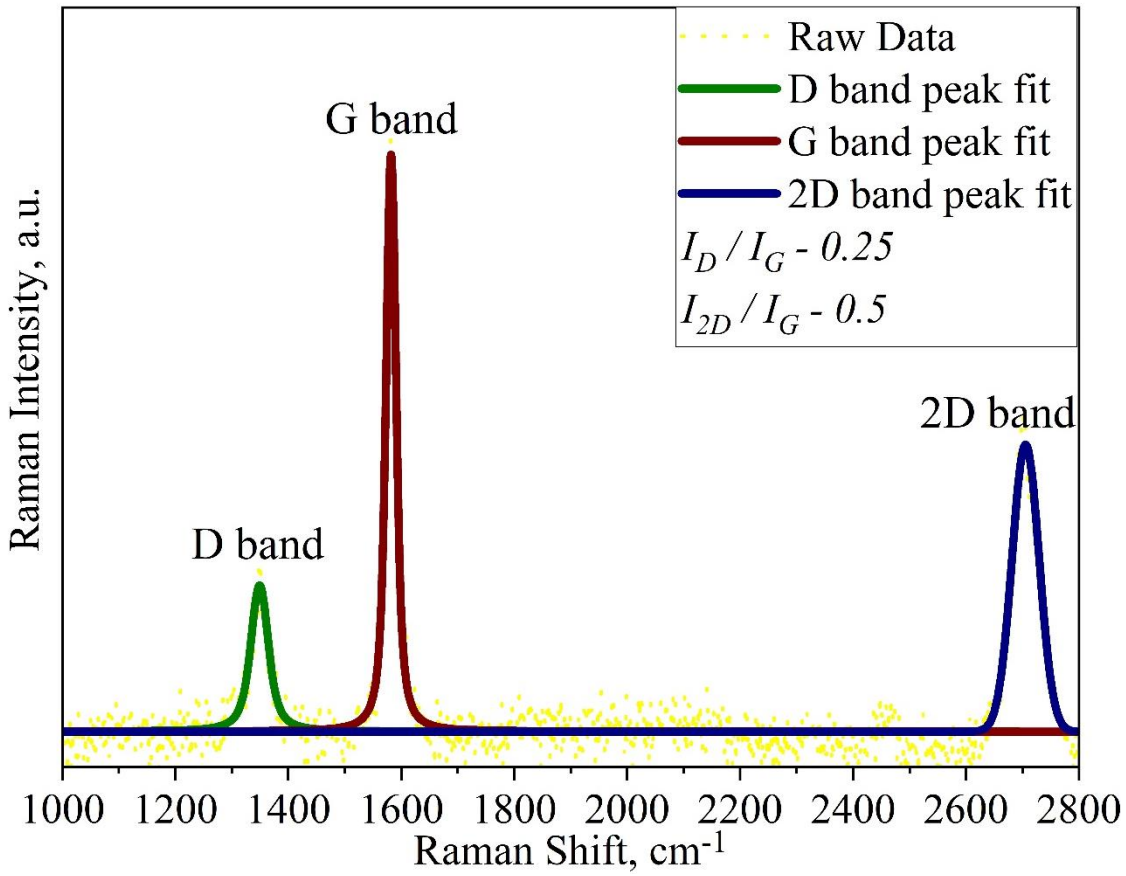

Figure 3. *Raman spectrum of chemical vapor deposited graphene*

The defects in graphene arise due to the in-plane cavities (during CVD growth), resulting in augmented edge formation in the graphene sheet. It is favorable for energy storage applications as it enhances the surface area, facile intercalation and deintercalation of electrolyte ions leading to better electrochemical performance [26]. It is well established from the previously reported research articles that the number of graphene layers in the sample can be estimated utilizing the normalized intensity ratio of the 2D-band (due to the second overtone of a different in-plane vibration) to the G-band (I_{2D}/I_G). If the I_{2D}/I_G ratio of greater than 2 is considered for monolayer graphene and I_{2D}/I_G ratio of 0.5 is considered for less than five-layer formation in graphene samples [46]. I_{2D}/I_G ratio in the graphene samples was found to be ≈0.5, indicating the formation of few-layer graphene.

FESEM analysis

Scanning electron microscopy images (shown in Figure 4a) were obtained for chemical vapor deposited graphene on copper foil samples, using FEI, Nova NanoSEM 450. Wrinkled micro-island formation of graphene can be easily visualized in the samples. These wrinkles increase electrochemically active surface area of graphene for charge storage [47]. At the same time, the

island formation in graphene supports the swift movement of electrolyte ions inside the electrode material and the availability of inner layers of graphene for charge storage leading to enhanced electrochemical performance [48]. The EDS mapping image of carbon (shown in Figure 4c) shows the uniformity of graphene on the copper catalyst. The presence of oxygen in the sample may be due to the oxidation of copper foil in the ambient atmosphere.

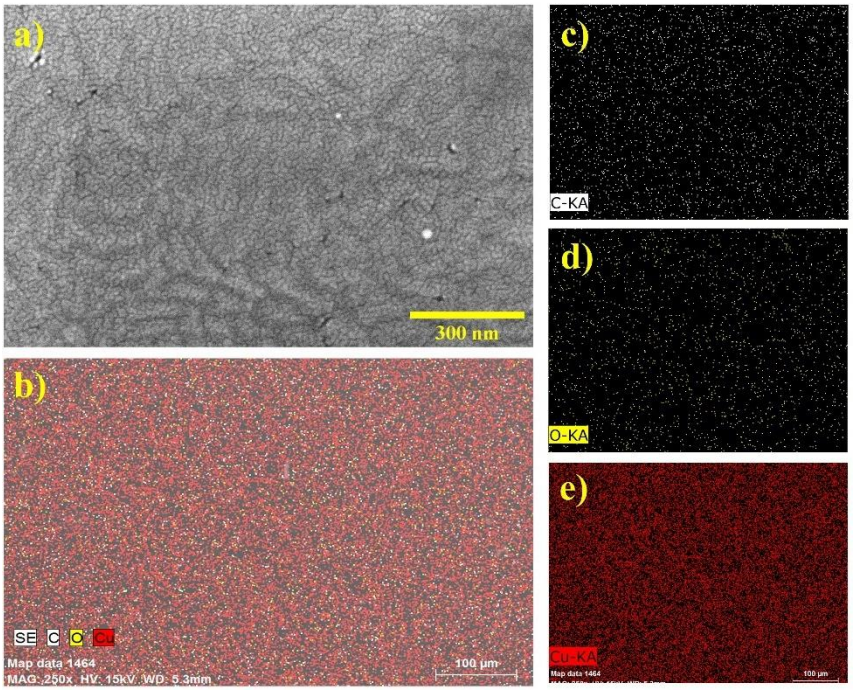

Figure 4. *a) FESEM image of CVD deposited graphene on copper b) EDS mapping image of carbon, oxygen and copper in CVD deposited graphene on copper c) EDS mapping image of carbon in CVD deposited graphene on copper d) EDS mapping image of oxygen in CVD deposited graphene on copper and e) EDS mapping image of copper in CVD deposited graphene on copper*

TEM analysis

TEM images (Figure 5) of the CVD deposited graphene were acquired using Tecnai G2 20 S-TWIN [FEI] HRTEM instrument. Restacking in multilayer graphene is a well-known setback that originated due to the van der Waals interactions among the graphene sheets. Van der Waals force is directly proportional to the surface area of sheet overlapping and inversely proportional to the square of the interlayer distance [49]. Restacking in graphene can be evaded in perforated or holey graphene owing to the deficiency of sufficient carbon atoms resulting in the lack of enough van der Waals forces. The reduced restacking and the existence of a large number of holes could result in a superior ionic approach to the surfaces, thus enhancing the available electrochemical surface area. The accessibility to a large number of perforations and increased interspacing between layers improve ionic diffusion and affluent mass transport [50]. This opens up a significant application of holey graphene in electrochemical energy storage. The TEM images reveal few-layer perforated graphene films with wrinkles, multiple creasing, and perforations that arise due to the hydrogen annealing of the copper catalyst and hydrogen etching of graphene [19,51]. The perforation in the graphene films provides facile back-and-forth passage of anions and cations throughout the electrode material, whereas the wrinkles and multiple creasing in graphene will provide enhanced surface area, resulting in excellent electrochemical performance [52,53].

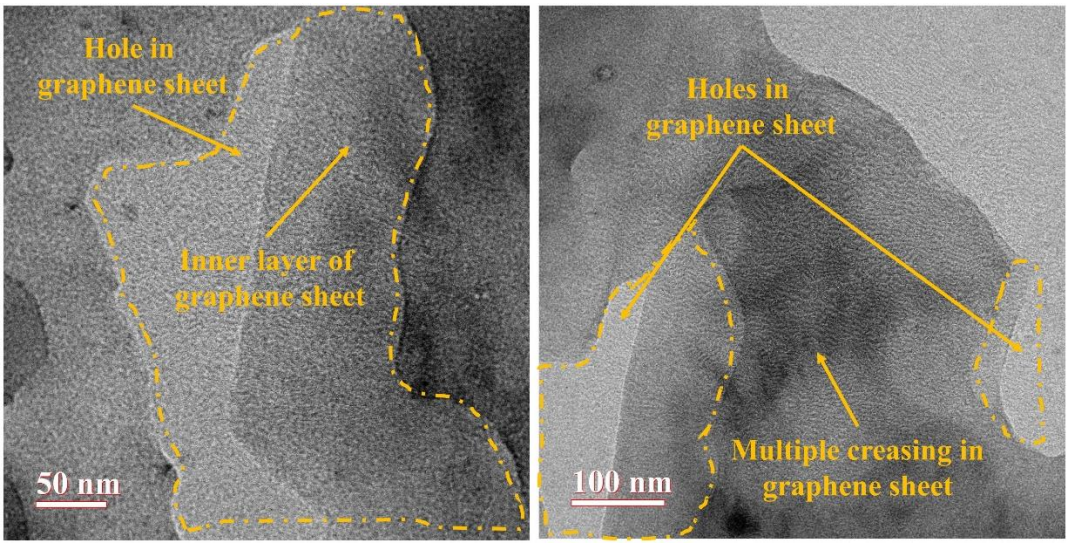

Figure 5. *TEM images of CVD deposited graphene transferred on the copper grid*

Electrochemical characterizations and analysis

To evaluate the merits of utilizing flexible electrodes in the device to form wearable and bendable electronics devices such as SCs, the SC performance of graphene transferred silver-coated PET substrate as an electrode was investigated. The graphene nanosheet was uniformly aggregated onto a silver-coated PET substrate. The used (graphene-transferred silver-coated PET substrate) electrode has a coarse and creased surface with a large number of holes. For the ultrathin and flexible supercapacitor device fabrication, the few-layer graphene was transferred onto the silver-coated PET substrates, and 1M Na_2SO_4 soaked PVA membranes were used as the separator-less quasi solid-state electrolyte. The CV curves illustrate the typical quasi-rectangular shape profiles at all scan rates as an indication of charge storage due to EDLC or intercalation capacitance. The cyclic voltammetry (CV) profile of the fabricated supercapacitor device (Figure 6a) was obtained at progressive scan rates (10-500 mV/s) and within the potential range of 0 – 1 V, no redox peaks were seen that accentuate no involvement of any Faradic dominated reactions in the charge-storage kinetics of graphene electrode.

Galvanostatic charge-discharge (GCD) curves (Figure 6b) at different current densities (0.05-0.5 mA cm^{-2}) show a nearly triangular shape for the fabricated device. It Indicates that the fabricated SC exhibit excellent capacitive behavior and high cyclic stability. The specific areal capacitance values for the fabricated SCs were calculated based on the equation –

$$C_S = \frac{4I\Delta t}{A\Delta V} \quad (1)$$

where I is the discharge current, Δt is the time of discharge, ΔV is the operating potential window, and A is the area of a single electrode [54]. The total area of the single electrode was 4 cm^2.

The specific areal capacitance of the fabricated flexible SCs was obtained as 15.3 mF cm^{-2} at the current density of 0.05 mA cm^{-2}. To the best of our knowledge, the reported capacitance value is superior in comparison to the previously reported CVD-based graphene supercapacitors [55-59]. The device exhibited good capacitance retention at high current densities (as shown in figure 6d) with respect to the specific capacitance at the current density of 0.05 mA cm^{-2}. The specific capacitance retention of 93.6, 84.9 and 78.4 % was calculated at the current density of 0.1, 0.25 and 0.5 mA cm^{-2}, respectively. The energy density values of 0.53, 0.50, 0.45 and 0.42 μWh cm^{-2} at a power density of 25, 50, 125 and 250 μW cm^{-2}, respectively. In Figure 6c, the cyclic stability and Coulombic efficiency of the

flexible device are shown as 87.73 and 97.03 %, respectively. This extraordinary electrochemical performance for both the power and energy densities of the flexible supercapacitor device indicates that the wrinkles and holey structure of the graphene and silver coated flexible PET substrate promotes a synergistic role in minimizing the internal resistance due to efficient intercalation-deintercalations of ions and intact electrode – current collector contact.

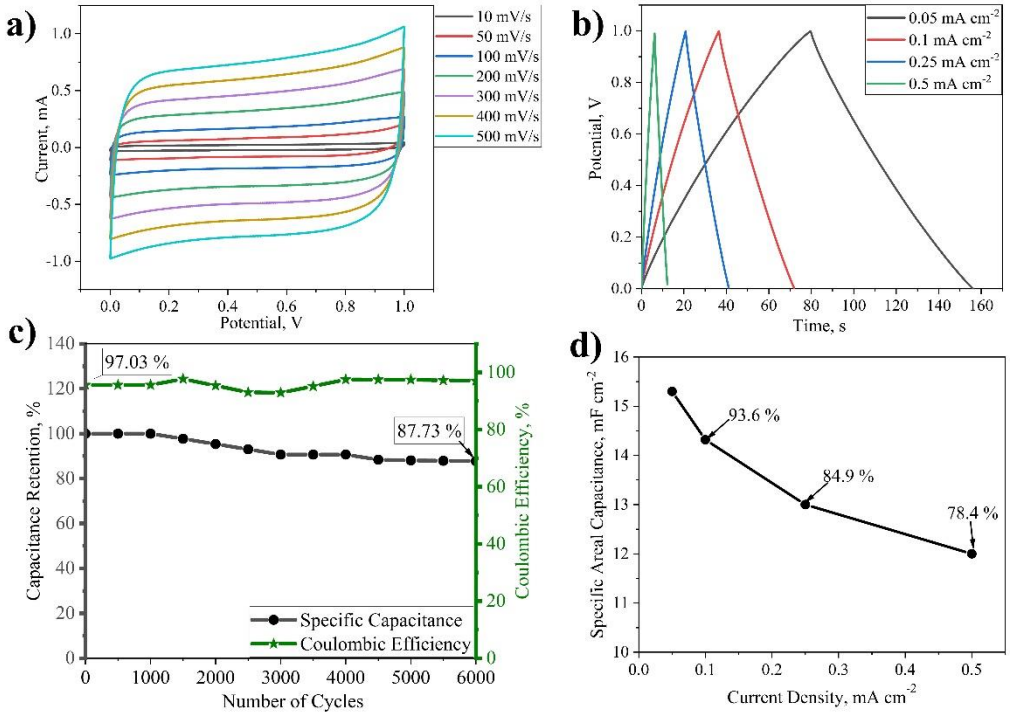

Figure 6. *a) CV plot of the flexible device at multiple scan rates (10-500 mV s^{-1}), b) GCD plot of the flexible device at various current densities (0.05 – 0.5 mA cm^{-2}), c) capacitance retention and Coulombic efficiency versus number of cycles plot of the fabricated flexible device, d) plot of specific capacitance versus current density of the fabricated SC device*

The EIS measurement (Figure 7a) was executed between 500 kHz and 0.01 Hz with an amplitude of 10 mV. In the case of an ideal capacitor, the phase shift angle of the impedance is perpendicular (θ ≈90°). Consequently, the nearly vertical impedance in the Nyquist plots of these ultrathin and flexible SC devices validates their performance as ideal capacitors. From the definition of the traditional capacitor, the capacitor impedance at high and low frequencies tends to be minimum (zero) and infinity, respectively [60]. Thus, at the higher frequency (500 kHz), the impedance of the supercapacitor device decreases steeply and will act as a short circuit resulting in the charge flow through ESR (equivalent circuit resistance) voluntarily and the phase angle comes to zero. This implies that the phase angle between voltage and current in an absolute resistor is zero. Nevertheless, at smaller frequencies (≈10 Hz), the capacitor impedance is sufficient enough to act as an open circuit. Consequently, at lower frequencies, the vital charge flow occurs through R_{ct} (charge transfer resistance) rather than ESR, therefore, R_{ct} will be the primary contributor to the device function [60]. The series and charge transfer resistances (R_{ct} were found to be 0.38 and 1.2 Ω, respectively, indicating free ionic movement at the electrode-electrolyte interface resulting in overall low resistance of the device.

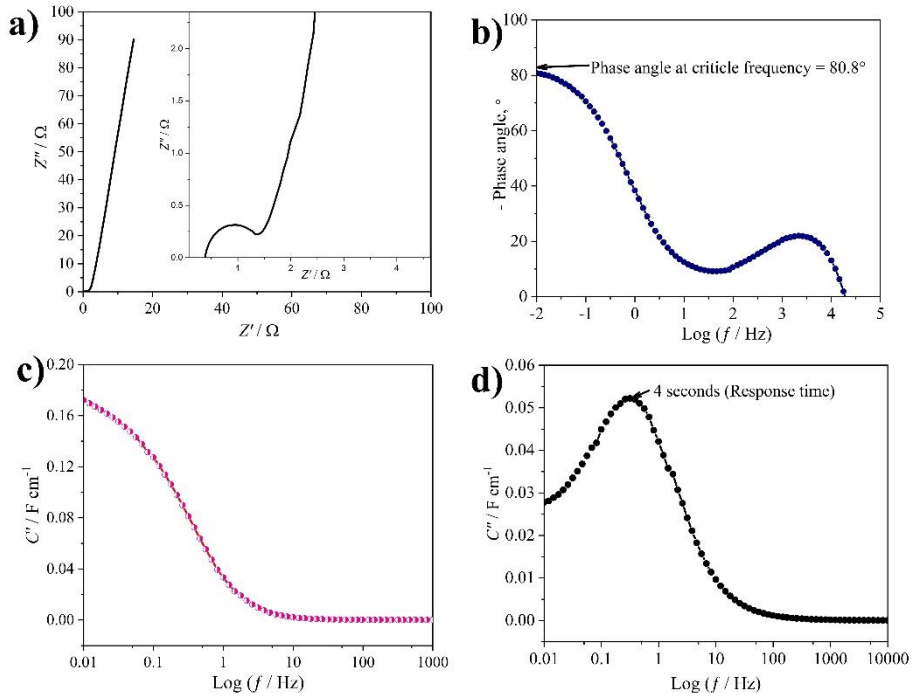

Figure 7. *a) Nyquist plot of the SC device, b) phase angle based Bode plot, c) real part of specific capacitance of SC device, d) imaginary part of specific capacitance of SC device.*

A supercapacitor impedance characteristics lie between an absolute resistor at phase angle 0° and an ideal capacitor at phase angle 90° [61]. The frequency is inversely proportional to capacitance, leading to almost zero impedance for a capacitor which results in an absolute resistor behavior at high frequencies [61]. Physical parameters like morphology, porosity, the thickness of the electrode, *etc.*, influence intermediate regions of frequencies that control the electrolyte ions diffusion at the electrode-electrolyte interface and inside the electrode material. The Bode plot of the flexible supercapacitor is shown in Figure 7b. Phase magnitude denotes the phase angle between the charging current and the voltage. For ideal supercapacitors, the magnitude possesses a phase angle of -90°. From the Bode plot (as shown in Figure 7b), the phase angle decreases sharply at critical frequency. In our case, the critical frequency magnitude of ~10 Hz with a phase angle of ~ -80.8° was observed, indicating that this device is very close to the ideal supercapacitive behavior.

For calculating the capacitive reactance of a capacitor from the Bode plot, equation (2) [62]-

$$X_c = \frac{1}{2\pi fC} \tag{2}$$

where X_c is capacitive reactance, and f denotes AC frequency.

For the Bode plot, the real capacitance was measured using equation (3) [62]

$$C'(\omega) = \frac{Z''(\omega)}{\omega\left|Z(\omega)\right|^2} \tag{3}$$

For the Bode plot, the imaginary capacitance was measured using equation (4) [62]

$$C''(\omega) = \frac{Z'(\omega)}{\omega\left|Z(\omega)\right|^2} \tag{4}$$

where $\omega=2\pi f$, Z' is real impedance, and Z'' is imaginary impedance.

For calculating the response time (τ_0), equation (5)

$$\tau_0 = \frac{1}{f_0} \quad (5)$$

where, f_0 is the frequency for which the imaginary part of the capacitance is maximum.

Figure 7c and figure 7d represent changes in the real (*C*') and imaginary part (*C*'') of capacitance versus the logarithm of frequency, respectively. According to the previous description, as frequency decreases, capacitance increases in the case of real capacitance and tends to be less frequency-dependent. This relation shows characteristics of electrode and electrode-electrolyte interface [63] and implies that the fabricated device is frequency-independent which makes it a strong candidate for AC filtering applications demanding ultrathin and flexible devices. However, the imaginary part of the capacitance attains a maximum value corresponding to a specific value of frequency which gives the response time of the device. By using the above equation (equation 5), response time is calculated as 4 seconds for the flexible SC device, which indicates the device can undergo ultrafast charging-discharging cycles.

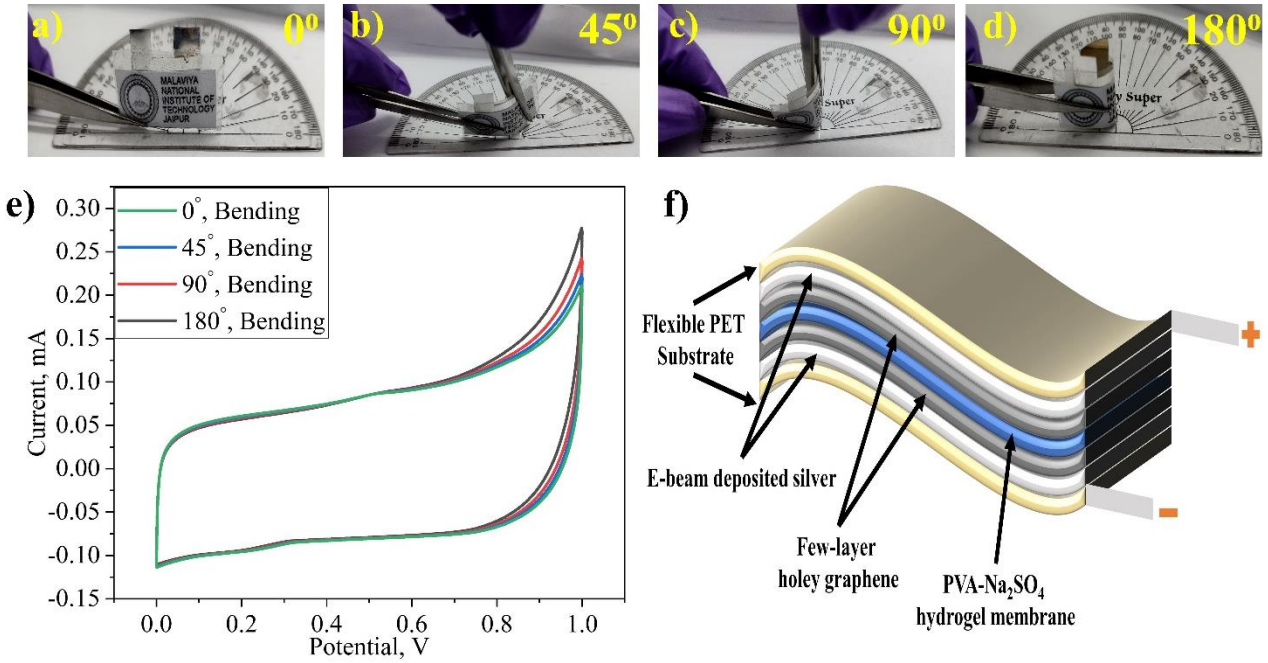

Figure 8. *a) Flexible supercapacitor device without bending (0°), b) flexible supercapacitor device with 45° bending, c) flexible supercapacitor device with 90° bending, d) flexible supercapacitor device with 180° bending, e) CV curves (at 50 mV s^{-1}) of the flexible supercapacitor device at 0°, 45°, 90° and 180° bending, f) schematic of the flexible supercapacitor device*

Table 1. *Comparison of electrochemical results of this study with previously reported works.*

No.	Electrode material	Electrolyte	Substrate	C_{sp} / mF cm^{-2}	Energy density, nWh cm^{-2}	Power density, μWcm^{-2}	Ref.
1.	CVD-graphene	PVA-H_2SO_4	Graphite paper	11.1	1.24	24.5	[64]
2.	Au/graphene	H_3PO_4-PVA	-	0.0081	-	-	[65]
3.	Graphene/PDMS	PVA-H_2SO_4	-	0.00533	0.20	11.17	[66]
4.	CVD graphene	H_3PO_4-PVA	PET	0.0124	0.47	70	[67]
5.	CVD graphene	BMIM-PF_4	Stainless steel	0.29	-	-	[68]
6.	Graphene core sheath microfibers	PVA-H_2SO_4	-	1.7	0.17	100	[69]
7.	CNT/graphene fiber	1 M Na_2SO_4	Au/PET	0.98	-	-	[70]
8.	Few-layer CVD graphene	PVA-Na_2SO_4 Hydrogel membrane	Ag/PET	15.3 (at 0.05 mA cm^{-2})	0.53	25	This work

Table 1 shows a comparative study of previously reported few-layer graphene materials employed to serve as the supercapacitor electrode material. The proposed device configuration successfully outperformed the results of the previously reported materials. Graphite foil, stainless steel, and indium doped tin oxide (ITO) have been widely used as the current collector for fabricating graphene electrodes, but due to their limited flexibility, heavy wight and relatively poor conductivity, there are not suitable choices for ultrathin and flexible supercapacitors [71,72]. This investigation offers a new approach to the fabrication of highly flexible and cost-effective silver deposited PET current collectors for supercapacitors. Further, the utilization of PVA-Na_2SO_4 hydrogel electrolyte in the supercapacitor device enhances the device performance in terms of energy density, power density and long cycle stability [65]. The flexible supercapacitor device demonstrated outstanding mechanical durability under several stress conditions, confirming its applicability in real applications. Figure 8e shows the cyclic voltammetry of the quasi-solid-state supercapacitor device without bending and under various bending conditions. The area of the single electrode of the device was 4 cm^2 and the bending was done in the middle region of the supercapacitor device. Under static bending, the area of the CV curve slightly increases due to the stretching and compression of hydrogel membrane electrolyte and the increment predominantly occurs in the pseudocapacitive region. It can be clearly observed that the CV curves show insignificant change due to stable connections between the silver current collector, graphene layers and hydrogel membrane electrolyte under all the bending conditions (0 – 180°), representing the robust, flexible operation of the supercapacitor [73]. Figure 8f shows a schematic diagram of the device, illustrating the LPCVD grown few-layer graphene transferred on E-beam deposited silver PET substrate (flexible current collector) sandwiched by a separator-less quasi-solid-state hydrogel membrane.

Conclusions

To summarize, we have been successful in developing lightweight and flexible SC using chemical vapor deposited a few layers of holey graphene. The E-beam deposition of silver on PET substrates provides an excellent substitute for the metallic conductors and the use of polymer gel membranes in the device leads to the ultrathin and quasi-solid-state device architecture. The device shows extraordinary mechanical stability under various bending conditions. The fabricated flexible SCs demonstrated an excellent specific areal capacitance of 15.3 mF cm^{-2} with an energy density and power density of 0.53 μWh cm^{-2} and 25 μW cm^{-2}, respectively, at the current density of 0.05 mA cm^{-2}. The outstanding performance of the fabricated ultrathin and flexible SC can be explained as: 1) the holey structure of graphene allows rapid movement of ions in the electrode material and makes the inner graphene layers accessible for charge storage, 2) the wrinkles and multiple creasing in the graphene has improved the theoretical electrochemical surface area for charge storage, leading to enhanced SC performance, 3) significant defect density in the graphene samples permits the prompt transport of large sodium ions.

Conflict of interest: *The authors express no conflict of interest.*

Acknowledgments: *The authors express their gratitude to the Materials Research Centre, MNITJ, for providing characterization facilities.*

References

[1] Y. Wang, X. Wu, Y. Han, T. Li, *Journal of Energy Storage* **42** (2021) 103053. https://doi.org/10.1016/j.est.2021.103053

[2] J. H. Yoon, Y. A. Kumar, S. Sambasivam, S. A. Hira, T. N. V. Krishna, K. Zeb, W. Uddin, K. D. Kumar, I. M. Obaidat, S. Kim, H. J. Kim, *Journal of Energy Storage* **32** (2020) 101988. https://doi.org/10.1016/j.est.2020.101988
[3] M. R. Pallavolu, Y. Anil Kumar, G. Mani, R. A. Alshgari, M. Ouladsmane, S. W. Joo, *Journal of Electroanalytical Chemistry* **899** (2021) 115695. https://doi.org/10.1016/j.jelechem.2021.115695
[4] D. K. Kulurumotlakatla, A. K. Yedluri, H. J. Kim, *Journal of Energy Storage* **31** (2020) 101619. https://doi.org/10.1016/j.est.2020.101619
[5] Y. A. Kumar, K. D. Kumar, H. J. Kim, *Dalton Transactions* **49** (2020) 3622-3629. https://doi.org/10.1039/d0dt00268b
[6] Y. A. Kumar, S. Singh, D. K. Kulurumotlakatla, H. J. Kim, *New Journal of Chemistry* **44** (2019) 522-529. https://doi.org/10.1039/c9nj05529k
[7] N. R. Reddy, P. M. Reddy, T. K. Mandal, A. K. Yedluri, S. W. Joo, *Journal of Energy Storage* **43** (2021) 103302. https://doi.org/10.1016/j.est.2021.103302
[8] Y. A. Kumar, S. Sambasivam, S. A. Hira, K. Zeb, W. Uddin, T. N. V. Krishna, K. D. Kumar, I. M. Obaidat, H. J. Kim, *Electrochimica Acta* **364** (2020) 137318. https://doi.org/10.1016/j.electacta.2020.137318
[9] Y. A. Kumar, K. D. Kumar, H. J. Kim, *Electrochimica Acta* **330** (2020) 135261. https://doi.org/10.1016/j.electacta.2019.135261
[10] Y. A. Kumar, K. D. Kumar, H. J. Kim, *Dalton Transactions* **49** (2020) 4050-4059. https://doi.org/10.1039/d0dt00191k
[11] Y. A. Kumar, H. J. Kim, *New Journal of Chemistry* **42** (2018) 19971-19978. https://doi.org/10.1039/c8nj05401k
[12] A. K. Yedluri, D. K. Kulurumotlakatla, S. Sangaraju, I. M. Obaidat, H. J. Kim, *Journal of Energy Storage* **31** (2020) 101623. https://doi.org/10.1016/j.est.2020.101623
[13] A. K. Thakur, K. Kurtyka, M. Majumder, X. Yang, H. Q. Ta, A. Bachmatiuk, L. Liu, B. Trzebicka, M. H. Rummeli, *Advanced Materials Interfaces* **9** (2022) 2101964. https://doi.org/10.1002/admi.202101964
[14] X. Huang, Z. Yin, S. Wu, X. Qi, Q. He, Q. Zhang, Q. Yan, F. Boey, H. Zhang, *Small* **7** (2011) 1876-1902. https://doi.org/10.1002/smll.201002009
[15] Q. Xiang, J. Yu, M. Jaroniec, *Chemical Society Reviews* **41** (2012) 782-796. https://doi.org/10.1039/c1cs15172j
[16] M. D. Stoller, S. Park, Y. Zhu, J. An, R. S. Ruoff, *Nano Letters* **8** (2008) 3498-3502. https://doi.org/10.1021/nl802558y
[17] Y. Wang, Y. Zheng, X. Xu, E. Dubuisson, Q. Bao, J. Lu, K. P. Loh, *ACS Nano* **5** (2011) 9927-9933. https://doi.org/10.1021/nn203700w
[18] D. A. C. Brownson, C. E. Banks, *Physical Chemistry Chemical Physics* **14** (2012) 8264-8281. https://doi.org/10.1039/c2cp40225d
[19] M. Losurdo, M. M. Giangregorio, P. Capezzuto, G. Bruno, *Physical Chemistry Chemical Physics* **13** (2011) 20836-20843. https://doi.org/10.1039/c1cp22347j
[20] S. Palsaniya, A. K. Dasmahapatra, *Graphene Supercapacitor Electrode of Liquid Hydrocarbons using CVD Process*, in: 2022 International Conference for Advancement in Technology, ICONAT 2022, Institute of Electrical and Electronics Engineers Inc., 2022. https://doi.org/10.1109/ICONAT53423.2022.9725983
[21] G. Gawlik, P. Ciepielewski, J. M. Baranowski, *Applied Sciences (Switzerland)* **9** (2019) 544. https://doi.org/10.3390/app9030544
[22] I. Vlassiouk, M. Regmi, P. Fulvio, S. Dai, P. Datskos, G. Eres, S. Smirnov, *ACS Nano* **5** (2011) 6069-6076. https://doi.org/10.1021/nn201978y

[23] Y. S. No, H. K. Choi, J. S. Kim, H. Kim, Y. J. Yu, C. G. Choi, J. S. Choi, *Scientific Reports* **8** (2018) 571. https://doi.org/10.1038/s41598-017-19084-1
[24] A. K. Nair, Indu Elizabeth, Gopukumar S., S. Thomas, Kala M. S, N. Kalarikkal, *Applied Surface Science* **428** (2018) 1119-1129. https://doi.org/10.1016/j.apsusc.2017.09.214
[25] Y. T. Liu, P. Zhang, N. Sun, B. Anasori, Q. Z. Zhu, H. Liu, Y. Gogotsi, B. Xu, *Advanced Materials* **30** (2018) 1707334. https://doi.org/10.1002/adma.201707334
[26] J. H. Jeong, G. W. Lee, Y. H. Kim, Y. J. Choi, K. C. Roh, K. B. Kim, *Chemical Engineering Journal* **378** (2019) 122126. https://doi.org/10.1016/j.cej.2019.122126
[27] F. Meng, T. Long, B. Xu, Y. Zhao, Z. Hu, L. Zhang, J. Liu, *Frontiers in Chemistry* **8** (2020) 652. https://doi.org/10.3389/fchem.2020.00652
[28] F. Rahmanabadi, P. Sangpour, A. A. Sabouri-Dodaran, *Journal of Electronic Materials* **48** (2019) 5813-5820. https://doi.org/10.1007/s11664-019-07361-w
[29] L. Gao, S. Chen, L. Zhang, X. Yang, *Journal of Alloys and Compounds* **766** (2018) 284-290. https://doi.org/10.1016/j.jallcom.2018.06.288
[30] W. Ye, H. Wang, J. Ning, Y. Zhong, Y. Hu, *Journal of Energy Chemistry* **57** (2021) 219-232. https://doi.org/10.1016/j.jechem.2020.09.016
[31] S. Alipoori, S. Mazinani, S. H. Aboutalebi, F. Sharif, *Journal of Energy Storage* **27** (2020) 101072. https://doi.org/10.1016/j.est.2019.101072
[32] J. Wang, G. Chen, S. Song, *Electrochimica Acta* **330** (2020) 135322. https://doi.org/10.1016/j.electacta.2019.135322
[33] A. K. Yedluri, H. J. Kim, *Dalton Transactions* **47** (2018) 15545-15554. https://doi.org/10.1039/c8dt03598a
[34] L. Ma, R. Liu, H. Niu, M. Zhao, Y. Huang, *Composites Science and Technology* **137** (2016) 87-93. https://doi.org/10.1016/j.compscitech.2016.10.027
[35] M. T. de A. Freire, A. P. Damant, L. Castle, F. G. R. Reyes, *Packaging Technology and Science* **12** (1999) 29-36. https://doi.org/10.1002/(SICI)1099-1522(199901/02)12:1%3C29::AID-PTS451%3E3.0.CO;2-D
[36] M. G. Faraj, K. Ibrahim, M. K. M Ali, *Optoelectronics and Advanced Materials-Rapid Communications* **5** (2011) 879-882. https://www.researchgate.net/publication/224880095
[37] I. Prosyčevas, J. Puišo, S. Tamulevičius, A. Juraitis, M. Andrulevičius, B. Čyžiūte, *Thin Solid Films* **495** (2006) 118-123. https://doi.org/10.1016/j.tsf.2005.08.278
[38] A. I. Oje, A. A. Ogwu, M. Mirzaeian, A. M. Oje, N. Tsendzughul, *Applied Surface Science* **488** (2019) 142-150. https://doi.org/10.1016/j.apsusc.2019.05.101
[39] K. S. Kim, H. J. Lee, C. Lee, S. K. Lee, H. Jang, J. H. Ahn, J. H. Kim, H. J. Lee, *ACS Nano* **5** (2011) 5107-5114. https://doi.org/10.1021/nn2011865
[40] R. Zan, A. Altuntepe, *Journal of Molecular Structure*. **1199** (2020) 127026. https://doi.org/10.1016/j.molstruc.2019.127026
[41] Y. Hwangbo, C. K. Lee, S. M. Kim, J. H. Kim, K. S. Kim, B. Jang, H. J. Lee, S. K. Lee, S. S. Kim, J. H. Ahn, S. M. Lee, *Scientific Reports* **4** (2014) 4439. https://doi.org/10.1038/srep04439
[42] Y. P. Hsieh, Y. W. Wang, C. C. Ting, H. C. Wang, K. Y. Chen, C. C. Yang, *Journal of Nanomaterials* **2013** (2013) 393724. https://doi.org/10.1155/2013/393724
[43] L. M. Malard, M. A. Pimenta, G. Dresselhaus, M. S. Dresselhaus, *Physics Reports* **473** (2009) 51-87. https://doi.org/10.1016/j.physrep.2009.02.003
[44] R. Beams, L. Gustavo Cançado, L. Novotny, *Journal of Physics: Condensed Matter* **27** (2015) 083002. https://doi.org/10.1088/0953-8984/27/8/083002
[45] J. B. Wu, M. L. Lin, X. Cong, H. N. Liu, P. H. Tan, *Chemical Society Reviews* **47** (2018) 1822-1873. https://doi.org/10.1039/c6cs00915h

[46] A. C. Ferrari, J. C. Meyer, V. Scardaci, C. Casiraghi, M. Lazzeri, F. Mauri, S. Piscanec, D. Jiang, K. S. Novoselov, S. Roth, A. K. Geim, *Physical Review Letters* **97** (2006) 187401. https://doi.org/10.1103/PhysRevLett.97.187401
[47] Z. Li, W. Zhang, J. Guo, B. Yang, J. Yuan, *Vacuum* **117** (2015) 35-39. https://doi.org/10.1016/j.vacuum.2015.03.032
[48] T. Chen, Y. Xue, A. K. Roy, L. Dai, *ACS Nano* **8** (2014) 1039-1046. https://doi.org/10.1021/nn405939w
[49] N. S. Rajput, S. Al Zadjali, M. Gutierrez, A. M. K. Esawi, M. Al Teneiji, *RSC Advances* **11** (2021) 27381-27405. https://doi.org/10.1039/d1ra05157a
[50] X. Yang, J. Zhu, L. Qiu, D. Li, *Advanced Materials* **23** (2011) 2833-2838. https://doi.org/10.1002/adma.201100261
[51] Y. Zhang, H. Zhang, F. Li, H. Shu, Z. Chen, Y. Sui, Y. Zhang, X. Ge, G. Yu, Z. Jin, X. Liu, *Carbon* **96** (2016) 237-242. https://doi.org/10.1016/j.carbon.2015.09.041
[52] C. Feng, Z. Yi, L. F. Dumée, F. She, Z. Peng, W. Gao, L. Kong, *Carbon* **139** (2018) 672-679. https://doi.org/10.1016/j.carbon.2018.07.016
[53] S. Yan, G. Zhang, H. Jiang, F. Li, L. Zhang, Y. Xia, Z. Wang, Y. Wu, H. Li, *ACS Applied Materials and Interfaces* **11** (2019) 10736-10744. https://doi.org/10.1021/acsami.9b00274
[54] D. Kim, K. Lee, M. Kim, Y. Kim, H. Lee, *Electrochimica Acta* **300** (2019) 461-469. https://doi.org/10.1016/j.electacta.2019.01.141
[55] X. Zang, P. Li, Q. Chen, K. Wang, J. Wei, D. Wu, H. Zhu, *Journal of Applied Physics* **115** (2014) 024305. https://doi.org/10.1063/1.4861629
[56] M. Bláha, M. Bouša, V. Valeš, O. Frank, M. Kalbáč, *ACS Applied Materials and Interfaces* **13** (2021) 34686-34695. https://doi.org/10.1021/acsami.1c05054
[57] J. Ye, H. Tan, S. Wu, K. Ni, F. Pan, J. Liu, Z. Tao, Y. Qu, H. Ji, P. Simon, Y. Zhu, *Advanced Materials* **30** (2018) 1801384. https://doi.org/10.1002/adma.201801384
[58] J. J. Yoo, K. Balakrishnan, J. Huang, V. Meunier, B. G. Sumpter, A. Srivastava, M. Conway, A. L. Mohana Reddy, J. Yu, R. Vajtai, P. M. Ajayan, *Nano Letters* **11** (2011) 1423-1427. https://doi.org/10.1021/nl200225j
[59] P. Xu, J. Kang, J. B. Choi, J. Suhr, J. Yu, F. Li, J. H. Byun, B. S. Kim, T. W. Chou, *ACS Nano* **8** (2014) 9437-9445. https://doi.org/10.1021/nn503570j
[60] H. Ur Rehman, A. Shuja, M. Ali, I. Murtaza, H. Meng, *Journal of Energy Storage* **28** (2020) 101243. https://doi.org/10.1016/j.est.2020.101243
[61] M. Arunkumar, A. Paul, *ACS Omega* **2** (2017) 8039-8050. https://doi.org/10.1021/acsomega.7b01275
[62] N. O. Laschuk, E. B. Easton, O. V. Zenkina, *RSC Advances* **11** (2021) 27925-27936. https://doi.org/10.1039/d1ra03785d
[63] P. L. Taberna, P. Simon, J. F. Fauvarque, *Journal of The Electrochemical Society* **150** (2003) A292. https://doi.org/10.1149/1.1543948
[64] A. Ramadoss, K. Y. Yoon, M. J. Kwak, S. I. Kim, S. T. Ryu, J. H. Jang, *Journal of Power Sources* **337** (2017) 159-165. https://doi.org/10.1016/j.jpowsour.2016.10.091
[65] Y. Chen, X. Y. Fu, Y. Y. Yue, N. Zhang, J. Feng, H. B. Sun, *Applied Surface Science* **467-468** (2019) 104-111. https://doi.org/10.1016/j.apsusc.2018.10.093
[66] P. Xu, J. Kang, J. B. Choi, J. Suhr, J. Yu, F. Li, J. H. Byun, B. S. Kim, T. W. Chou, *ACS Nano* **8** (2014) 9437-9445. https://doi.org/10.1021/nn503570j
[67] Y. Gao, Y. S. Zhou, W. Xiong, L. J. Jiang, M. Mahjouri-Samani, P. Thirugnanam, X. Huang, M. M. Wang, L. Jiang, Y. F. Lu, *APL Materials* **1** (2013) 012101. https://doi.org/10.1063/1.4808242
[68] X. Zang, P. Li, Q. Chen, K. Wang, J. Wei, D. Wu, H. Zhu, *Journal of Applied Physics* **115** (2014) 024305. https://doi.org/10.1063/1.4861629

[69] Y. Meng, Y. Zhao, C. Hu, H. Cheng, Y. Hu, Z. Zhang, G. Shi, L. Qu, *Advanced Materials* **25** (2013) 2326-2331. https://doi.org/10.1002/adma.201300132
[70] H. Cheng, Z. Dong, C. Hu, Y. Zhao, Y. Hu, L. Qu, N. Chen, L. Dai, *Nanoscale* **5** (2013) 3428-3434. https://doi.org/10.1039/c3nr00320e
[71] G. K. Dalapati, H. Sharma, A. Guchhait, N. Chakrabarty, P. Bamola, Q. Liu, G. Saianand, A. M. Sai Krishna, S. Mukhopadhyay, A. Dey, T. K. S. Wong, S. Zhuk, S. Ghosh, S. Chakrabortty, C. Mahata, S. Biring, A. Kumar, C. S. Ribeiro, S. Ramakrishna, A. K. Chakraborty, S. Krishnamurthy, P. Sonar, M. Sharma, *Journal of Materials Chemistry A* **9** (2021) 16621-16684. https://doi.org/10.1039/d1ta01291f
[72] B. Hsia, M. S. Kim, L. E. Luna, N. R. Mair, Y. Kim, C. Carraro, R. Maboudian, *ACS Applied Materials and Interfaces* **6** (2014) 18413-18417. https://doi.org/10.1021/am504695t
[73] Y. Ko, M. Kwon, W. K. Bae, B. Lee, S. W. Lee, J. Cho, *Nature Communications* **8** (2017) 536. https://doi.org/10.1038/s41467-017-00550-3